Fast pseudo-CT synthesis from MRI T1-weighted images using a patch-based approach

A. Torrado-Carvajal*[ab], E. Alcain[c], A. S. Montemayor[c], J. L. Herraiz[b,d], Y. Rozenholc[e]
J. A. Hernandez-Tamames[a,b], E. Adalsteinsson[b,f,g,h], L. L. Wald[b,h,i], N. Malpica[a,b]

[a]Medical Image Analysis and Biometry Lab, Universidad Rey Juan Carlos, Mostoles, Madrid; [b]Madrid-MIT M+Vision Consortium, Madrid, Spain; [c]Dept. of Computer Science, Universidad Rey Juan Carlos, Mostoles, Madrid; [d]Research Laboratory of Electronics, Massachusetts Institute of Technology, Cambridge, Massachusetts, USA; [e]MAP5, CNRS UMR 8145, University Paris Descartes, Paris, Paris, France; [f]Dept. of Electrical Engineering and Computer Science, Massachusetts Institute of Technology, Cambridge, Massachusetts, USA; [g]Institute of Medical Engineering and Science, Massachusetts Institute of Technology, Cambridge, Massachusetts, USA; [h]Harvard-MIT Health Sciences and Technology, Massachusetts Institute of Technology, Cambridge, Massachusetts, USA; [i]A. A. Martinos Center for Biomedical Imaging, Dept. of Radiology, Massachusetts General Hospital, Charlestown, Massachusetts, USA

ABSTRACT

MRI-based bone segmentation is a challenging task because bone tissue and air both present low signal intensity on MR images, making it difficult to accurately delimit the bone boundaries. However, estimating bone from MRI images may allow decreasing patient ionization by removing the need of patient-specific CT acquisition in several applications. In this work, we propose a fast GPU-based pseudo-CT generation from a patient-specific MRI T1-weighted image using a group-wise patch-based approach and a limited MRI and CT atlas dictionary. For every voxel in the input MR image, we compute the similarity of the patch containing that voxel with the patches of all MR images in the database, which lie in a certain anatomical neighborhood. The pseudo-CT is obtained as a local weighted linear combination of the CT values of the corresponding patches. The algorithm was implemented in a GPU. The use of patch-based techniques allows a fast and accurate estimation of the pseudo-CT from MR T1-weighted images, with a similar accuracy as the patient-specific CT. The experimental normalized cross correlation reaches 0.9324±0.0048 for an atlas with 10 datasets. The high NCC values indicate how our method can accurately approximate the patient-specific CT. The GPU implementation led to a substantial decrease in computational time making the approach suitable for real applications.

Keywords: Bone detection, GPU processing, modality propagation, patch-based, pseudo-CT

1. INTRODUCTION

Skull segmentation from Magnetic Resonance Imaging (MRI) data is receiving a lot of attention, as there are many applications in which a precise delineation of the skull is needed. Accurate construction of patient-specific tissue models for dosimetry applications in electromagnetics[1] (EM), medical radiation physics[2], or the use of tissue information for attenuation correction in PET-MR[3],[4] are three of the most important examples.

Nevertheless, MRI-based bone segmentation, specifically automatic segmentation of the skull, is a challenging task. On one hand, bone tissue and air both present low signal intensity on MR images, making it difficult to accurately delimit the bone boundaries. On the other hand, the high complexity of the skull anatomy, its fuzzy boundaries and missing edge features hinders the application of general-purpose segmentation methods.

The development and implementation of the Ultra-short TE (UTE) sequences allowed detecting signal from previously unobservable tissues such as cortical bone, tendons, ligaments and menisci[5]. Keereman et al. proposed the use of the transverse relaxation rate derived from UTE images to classify the voxels into skull, soft tissue, and air[6].

11th International Symposium on Medical Information Processing and Analysis, edited by Eduardo Romero, Natasha Lepore, Juan D. García-Arteaga, Jorge Brieva, Proc. of SPIE Vol. 9681, 968106
© 2015 SPIE · CCC code: 0277-786X/15/$18 · doi: 10.1117/12.2210963

Rifai et al. proposed a 3D method for segmenting bone regions in MRI volumes using deformable models and taking the partial volume effect into account[7]. Wang et al. proposed the use of a CT database to create a reliable shape model used to locate the skull shape in MRI[8].

We previously proposed a method for complete skull segmentation based only on T1-weigthed images of the human head[9]. The skull was estimated using a multi-atlas segmentation and label-fusion approach. CTs from a whole head CT-scan database were registered to the patient MRI image using affine a non-rigid registration; then, the final patient-specific skull is estimated using label fusion techniques.

However, these methods present several limitations: methods based on UTE sequences have safety issues of high radio-frequency power being delivered into the patient's body; methods based on deformable models or label-fusion loose detail presenting smoothed contours of the skull as a result of the label-fusion volume averaging.

Recently, patch-based methods have showed to be a versatile segmentation technique[10], relaxing the one-to-one constraint existing in non-rigid registration. Several approaches have been introduced depending on the patch fusion methods or rules[11],[12]. Ye et al. proposed a patch-based method for generating a T2 volume from a T1-weighted volume[13].

In this work, we propose a method for fast pseudo-CT generation from a patient-specific MRI T1-weighted image using a group-wise patch-based approach on a MRI and CT atlas dictionary.

2. PATCH-BASED LABEL PROPAGATION

Patch-based segmentation was introduced as an alternate approach for label propagation, which eliminates the requirement of non-rigid registration[10]. This technique was developed as an adaptation of the non-local frameworks developments in non-local denoising[14],[15].

Let I be an input image to be processed, and A an anatomy atlas containing a set of MRI T1-weighted volumes I_{MR} and the corresponding CT volumes I_{CT}, so that $A=\{(I^i_{MR},I^i_{CT}),\ i=1,...,n\}$.

Weigths Estimation

Let us consider ω_i as a weight reflecting non-local similarities between voxels $\boldsymbol{a}=(a_x,a_y,a_z)$ in the input image I and voxels $\boldsymbol{b}=(b_x,b_y,b_z)$ in the image I^i_{MR} of the atlas A over the image domain Ω, and computed using the following equation:

$$w(a,b)=f\left(\frac{\sum_{a'\in P_I(a),b'\in P_{I^i_{MR}}(b)}\left(I(a')-I^i_{MR}(b')\right)^2}{2S\beta\hat{\sigma}^2}\right) \quad (1)$$

where $P_I(\boldsymbol{a})$ is a 3D patch of the image I centered at voxel $\boldsymbol{a}$, S is the number of voxels in the 3D patch; β is a smoothing parameter, and σ is the standard deviation of the noise. The original denoising approach assumes that similarities of a patch can be found over the entire image domain Ω. However, in the context of modality propagation, the variations of the anatomical structures in a population are bounded, so we can find good matches in a specific neighborhood $N(\boldsymbol{a})$ of a specific voxel $\boldsymbol{a}$. The weights are then estimated in this local area as $\omega=\{\omega(\boldsymbol{a},\boldsymbol{b}),\ \forall\, \boldsymbol{a}\in\Omega,\ \boldsymbol{b}\in N(\boldsymbol{a})\}$, reflecting the local similarities between I and I^i_{MR}. The size of the considered neighborhood N has been set to 11 in this paper, which is directly related to the head anatomical variability.

Group-Wise Label Propagation

Using equation 1 to calculate the weights, the image $I_{pseudoCT}$ can be estimated as follows:

$$\forall a \in \Omega,\ \ I_{pseudoCT}(a) = \frac{\sum_{i=1}^{n} \sum_{b \in N(a)} \omega(a,b) I_{CT}^{i}(b)}{\sum_{i=1}^{n} \sum_{b \in N(a)} \omega(a,b)} \tag{2}$$

Which takes all the images I^{i}_{MR} in the atlas A to produce a group-wise combination of I^{i}_{CT}, thus, obtaining an estimation of $I_{pseudoCT}$.

Regularization

Contrary to registration-based approaches, if there is no correspondence between the patch of the input image I and the patches of the images I^{i}_{MR} in the atlas A, no value (NaN) is asigned to the voxel $\boldsymbol{a}$ of $I_{pseudoCT}$.

This situation makes it necessary to include a regularization step dealing with non-labeled voxels. Usually these cases are isolated, so in this work we have assigned to this voxel the value of the median in its neighborhood. The size of the neighborhood $N_2(\boldsymbol{a})$ has been set to 3 in this paper.

$$\forall a = NaN \in \Omega,\ \ I_{pseudoCT}(a) = median_{N_2(a)}\left(I_{pseudoCT}(a)\right) \tag{3}$$

3. MATERIALS AND METHODS

MRI-CT data set

We have used a data set containing 19 healthy volunteers MRI-CT pairs to evaluate the patch-based pipeline. MRI images of the head were acquired on a General Electric Signa HDxt 3.0T MR scanner using the body coil for excitation and an 8-channel quadrature brain coil for reception. Subjects were positioned supine. Imaging was performed using an isotropic 3DT1w SPGR sequence with a TR=10.024ms, TE=4.56ms, TI=600ms, NEX=1, acquisition matrix=288x288, resolution=1x1x1mm, flip angle=12. CT images were acquired on a Siemens Somatom Sensation 16 CT scanner with matrix=512x512, resolution=0.48x0.48mm, slice thickness=0.75mm, PITCH=0.7mm, acquisition angle=0º, voltage=120kV, radiation intensity=200mA.

Image preprocessing was carried out using 3D Slicer built-in modules. This preprocessing included MRI bias correction (N4 ITK MRI bias correction), rigid registration (general registration BRAINS) to align all the images, and normalization of the grayscale values (ITK-based histogram matching).

This data set has been separated into an atlas A containing 10 MRI-CT pairs $A=\{(I^{i}_{MR},I^{i}_{CT}),\ i=1,...,10\}$, and a test set T containing the 9 remaining MRI-CT pairs $T=\{(I^{i}_{MR},I^{i}_{CT}),\ i=1,...,9\}$.

GPU Implementation

GPU Computing has gained importance to speed up algorithms in all scientific fields as well as in industry. The Patch-Based algorithm is highly parallelizable; our routine is comprised of ten loops: Three loops iterate through the 3D input image selecting a patch to be compared, the fourth loop it is used for selecting the atlas, the next three loops iterate through the neighborhood N selecting the atlas patch, the last three loops are in charge of the minimum square error calculation between both patches (input image and atlas).

The calculation of each point in the 3D image is completely independent from the others. Configuring a 3D grid in CUDA model allows eliminating the three external loops. Our CUDA kernel contains the rest of the loops and this way each label calculation is performed in a separate thread.

4. EXPERIMENTAL RESULTS

Qualitative results

Figure 1 shows the estimation result in the three planes (sagittal, coronal and axial) of a complete head MRI volume, the CT ground truth, and the estimated pseudo-CT for two healthy subjects. The proposed method approaches the shape of the skull generally well despite the patient-specific anatomical variations.

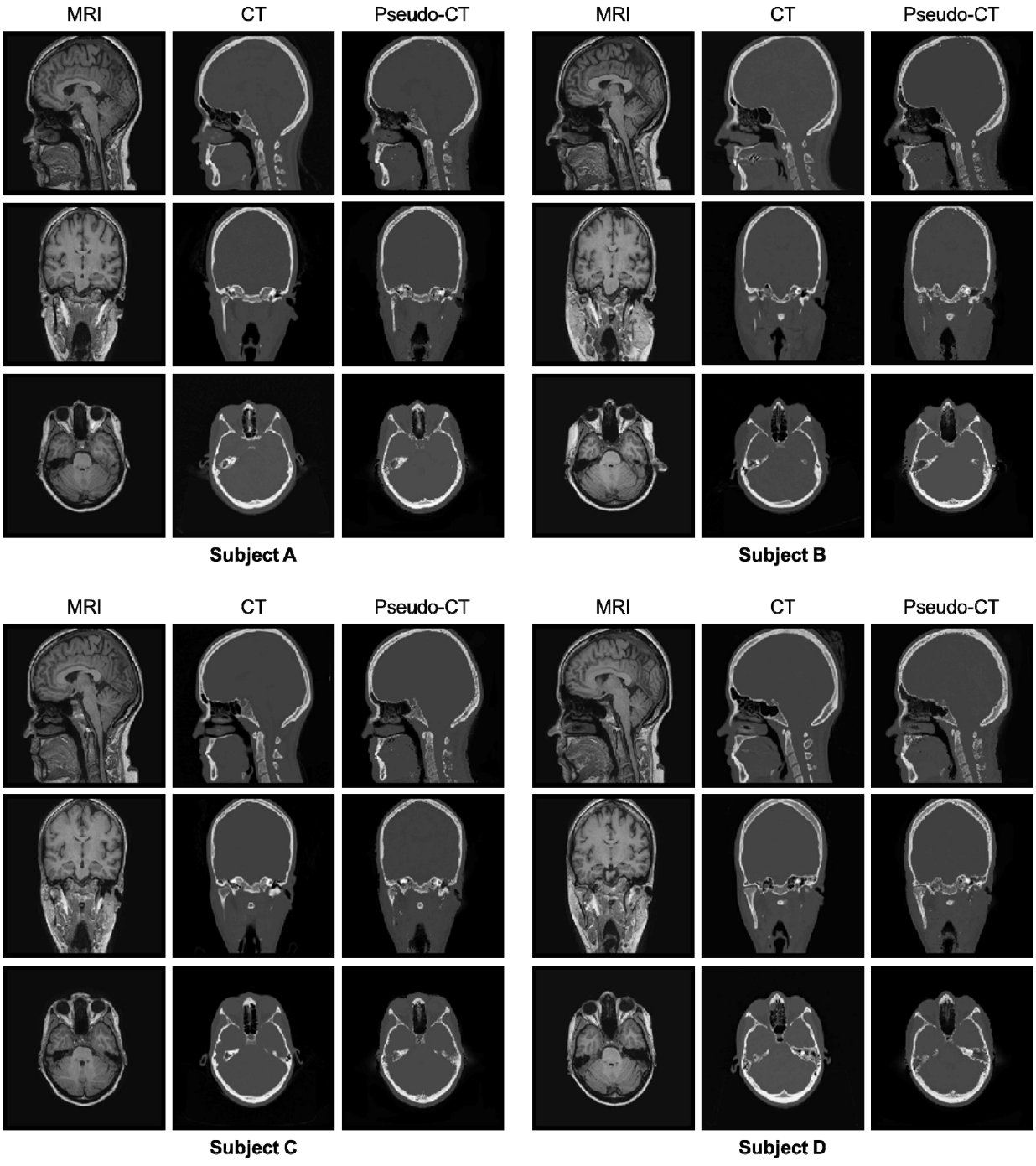

Figure 1. Three planes (sagittal, coronal and axial) of the MRI (first column), CT (second column), and pseudo-CT (third column) of a first subject, and MRI (fourth column), CT (fifth column), and pseudo-CT (sixth column) of a second subject.

The comparison between the patient-specific CT and the pseudo-CT shows how our method is able to approximate to the ground truth, delimiting the skull contours and differentiating air from bone. Visual inspection of the segmentation results shows the high quality of the pseudo-CT estimation and the robustness of the method, which is able to capture the details of the bone spikes in non-smooth areas such as the sinuses or the cervical vertebrae.

Quantitative results

We also tested the effect of changing the size of the atlas on the quality of the synthesized images in subjects without skull deformations, using atlas of 5, 7, and 10 datasets (Figure 2).

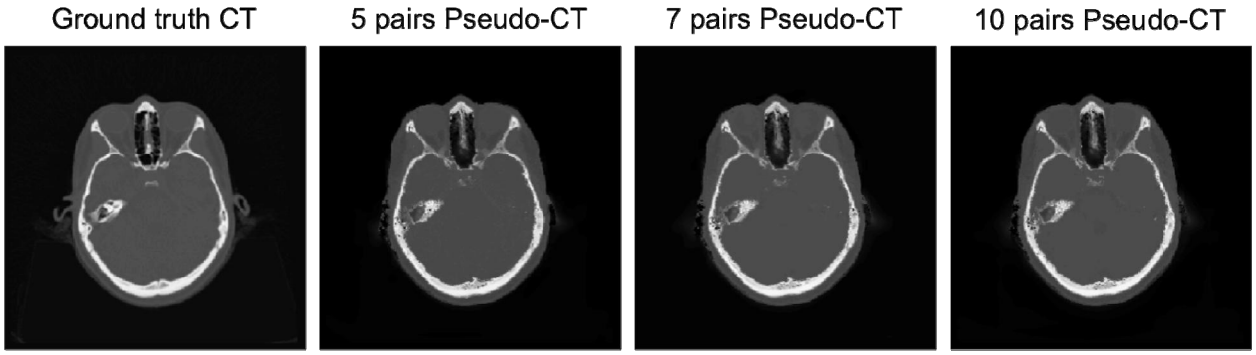

Figure 2. Axial plane of the patient specific (ground truth) CT and pseudo-CTs synthesized using atlases of different sizes.

We used the normalized cross correlation (NCC) to quantitatively measure the quality of the synthesized pseudo-CTs (I2) compared to the ground truth CT (I1) following equation 2.

$$NCC = \frac{1}{N}\sum_{x,y}\frac{\left(I_1(x,y)-\mu_1\right)\left(I_2(x,y)-\mu_2\right)}{\sigma_1\sigma_2} \tag{2}$$

The experimental NCC was 0.9281±0.0066 for the atlas with 5 datasets, 0.9294±0.0051 for the atlas with 7 datasets, and 0.9324±0.0048 for the atlas with 10 datasets. The high NCC values indicate how our method can accurately approximate the patient-specific CT.

Computational time

Table 1 shows the average computational time of the same algorithm implemented in different programming languages and using different configurations. The matrix size of the atlases, labels and the input volumes were 55x55x45 voxels. All matrices are represented in single precision. The time for GPU configuration includes the memory transfers (host to graphics card memory and viceversa).

In the worst-case scenario (10 atlases), computation of the pseudo-CT volume with the GPU implementation takes 4374 times less time than with the Matlab implementation, 27 times less than using the C implementation and 11 times less than with the C OpenMP version.

Table 1. Comparison of the average ± standard deviation of the computational time spent in processing 10 input volumes for each configuration. Matlab code was tested only once due to the computational cost. The C OpenMP implementation was configured to use 32 threads.

	Computational Time (seconds)			
# Atlases	**Matlab**	**C**	**C OpenMP**	**GPU**
5	8289.80	60.34 ± 0.02	31.08 ± 0.09	2.23 ± 0.00
7	11726.60	84.58 ± 0.04	37.41 ± 0.29	3.12 ± 0.00
10	19488.00	120.83 ± 0.14	50.24 ± 0.13	4.46 ± 0.00

All the experiments have been tested over Windows Server 2008 R2, on a Dual Intel Xeon-E5 2687W CPU processor @3.1GHz, using Matlab 2014a with MATLAB Parallel Toolbox. In addition to that, there is a NVIDIA Tesla K20X GPU card with 6GB dedicated memory.

5. CONCLUSIONS

In this paper we have presented a fast approach for the estimation of a pseudo-CT by using a multi-atlas and a patch-based approach based on a single T1-weighted MRI image of a subject as input. Constructing a pseudo-CT from an only MRI T1-weigthed acquisition is interesting to decrease patient ionization by removing the need of patient-specific CT acquisition while obtaining a good estimation of the actual CT. Additionally, the use of only MRI instead of MRI+CT has the advantage of decreasing costs and acquisition time, while allowing detailed information of soft tissues.

The approach performs successfully and could be very useful for tasks where the skull estimation is needed such as attenuation correction in hybrid PET/MR systems, and Specific Absorption Rate (SAR) calculations in high-field MRI.

Although the results of the computational times are very promising, this is a naive implementation. Most of accesses are from global memory; global memory accesses are 10x slower than shared memory. Future implementations will head this direction to speed up our proposal.

REFERENCES

[1] Homann, H., Graesslin, I., Eggers, H., Nehrke, K., Vernickel, P., Katscher, U., Dössel, O., Börnert, P., "Local SAR management by RF shimming: a simulation study with multiple human body models", Magn Reson Mater Phy, 25(3), 193-204 (2012).

[2] Andreo, P., "Monte Carlo techniques in medical radiation physics", Phys Med Biol, 36(7), 861-920 (1991).

[3] Martinez-Möller, A., Souvatzoglou, M., Delso, G., Bundschuh, R. A., Chefd'hotel, C., Ziegler, S. I., Navab, N., Schwaiger, M., Nekolla, S. G., "Tissue classification as a potential approach for attenuation correction in whole-body PET/MRI: evaluation with PET/CT data", J Nucl Med, 50(4), 520-526 (2009).

[4] Wagenknecht, G., Kaiser, H. J., Mottaghy, F. M., Herzog, H., "MRI for attenuation correction in PET: methods and challenges", Magn Reson Mater Phy, 26(1), 99-113 (2013).

[5] Robson, M. D., Bydder, G. M., "Clinical ultrashort echo time imaging of bone and other connective tissues", NMR Biomed, 19(7), 765-780 (2006).

[6] Keereman, V., Fierens, Y., Broux, T., De Deene, Y., Lonneux, M., Vandenberghe, S., "MRI-based attenuation correction for PET/MRI using ultrashort echo time sequences", J Nucl Med, 51(5), 812-818 (2010).

[7] Rifai, H., Bloch, I., Hutchinson, S., Wiart, J., Garnero, L., "Segmentation of the skull in MRI volumes using deformable model and taking the partial volume effect into account", Med Image Anal, 4(3), 219-233 (2000).

[8] Wang, D., Shi, L., Chu, W. C., Cheng, J. C., Heng, P. A., "Segmentation of human skull in MRI using statistical shape information from CT data", J Magn Reson Imaging, 30(3), 490-498 (2009).

[9] Torrado-Carvajal, A., Herraiz, J. L., Hernandez-Tamames, J. A., Jose-Estepar, S., Eryaman, Y., Rozenholc, Y., Adalsteinsson, E., Wald, L. L., Malpica, N., "Multi-atlas and label fusion approach for patient-specific MRI based skull estimation", Magn Reson Med, DOI: 10.1002/mrm.25737.
[10] Rousseau, F., Habas, P. A., Studholme, C., "A supervised patch-based approach for human brain labeling". IEEE T Med Imaging, 30(10), 1852-1862 (2011).
[11] Coupé, P., Manjón, J. V., Fonov, V., Pruessner, J., Robles, M., Collins, D. L., "Patch-based segmentation using expert priors: Application to hippocampus and ventricle segmentation", NeuroImage, 54(2), 940-954 (2011).
[12] Bai, W., Shi, W., O'Regan, D. P., Tong, T., Wang, H., Jamil-Copley, S., Peters, N. S., Rueckert, D., "A probabilistic patch-based label fusion model for multi-atlas segmentation with registration refinement: application to cardiac MR images", IEEE T Med Imaging, 32(7), 1302-1315 (2013).
[13] Ye, D. H., Zikic, D., Glocker, B., Criminisi, A., Konukoglu, E., "Modality propagation: coherent synthesis of subject-specific scans with data-driven regularization", Proc. MICCAI 2013, 606-613 (2013).
[14] Buades, A., Coll, B., Morel, J. M., "A review of image denoising algorithms, with a new one", Multiscale Model Sim, 4(2), 490-530 (2005).
[15] Katkovnik, V., Foi, A., Egiazarian, K., Astola, J., "From local kernel to nonlocal multiple-model image denoising". Int J Comput Vision, 86(1), 1-32 (2010).